Monthly Notices
of the
ROYAL ASTRONOMICAL SOCIETY

MNRAS **477,** 5682–5691 (2018)
Advance Access publication 2018 April 27

doi:10.1093/mnras/sty1069

Tidal disruption of inclined or eccentric binaries by massive black holes

Harriet Brown,[1]★ Shiho Kobayashi,[1] Elena M. Rossi[2] and Re'em Sari[3]

[1]*Astrophysics Research Institute, LJMU, IC2, Liverpool Science Park, 146 Brownlow Hill, Liverpool L3 5RF, UK*
[2]*Leiden University, Oort Building, Niels Bohrweg 2, NL-2333 CA Leiden, the Netherlands*
[3]*Racah Institute of Physics, Hebrew University, Jerusalem 91904, Israel*

Accepted 2018 April 24. Received 2018 April 2; in original form 2017 August 25

ABSTRACT

Binary stars that are on close orbits around massive black holes (MBHs) such as Sgr A* in the centre of the Milky Way are liable to undergo tidal disruption and eject a hypervelocity star. We study the interaction between such an MBH and circular binaries for general binary orientations and penetration depths (i.e. binaries penetrate into the tidal radius around the BH). We show that for very deep penetrators, almost all binaries are disrupted when the binary rotation axis is roughly oriented towards the BH or it is in the opposite direction. The surviving chance becomes significant when the angle between the binary rotation axis and the BH direction is between 0.15π and 0.85π. The surviving chance is as high as $\sim$20 per cent when the binary rotation axis is perpendicular to the BH direction. However, for shallow penetrators, the highest disruption chance is found in such a perpendicular case, especially in the prograde case. This is because the dynamics of shallow penetrators is more sensitive to the relative orientation of the binary and orbital angular momenta. We provide numerical fits to the disruption probability and energy gain at the BH encounter as a function of the penetration depth. The latter can be simply rescaled in terms of binary masses, their initial separation, and the binary-to-BH mass ratio to evaluate the ejection velocity of a binary members in various systems. We also investigate the disruption of coplanar, eccentric binaries by an MBH. It is shown that for highly eccentric binaries retrograde orbits have a significantly increased disruption probability and ejection velocities compared to the circular binaries.

Key words: methods: numerical – binaries: general – Galaxy: centre – Galaxy: kinematics and dynamics.

1 INTRODUCTION

Hypervelocity stars (HVSs) are stars with sufficient velocity to escape from the Galactic gravitational potential. Targeted HVS Surveys (Brown, Geller & Kenyon 2009, 2012, 2014) have led to the identification of 21 unbound stars to date. There are two main processes theorized to produce HVSs from the Galactic nucleus: the disruption of a binary system by a massive black hole (MBH) known as the Hills mechanism (Hills 1988), and three-body interaction between an MBH binary and an orbiting star (Yu & Tremaine 2003). For a binary with separation a and total mass m interacting with an MBH with mass M, the distance at which the tidal forces overcome the binary's self-gravity is about $r_t = a(M/m)^{1/3}$. According to the Hills mechanism, once the binary crosses the tidal radius and it is tidally disrupted, one of the binary members is ejected at high speeds of the order of $v_0(M/m)^{1/6} \sim 2000(\mathrm{m/M_\odot})^{1/3}(a/5\,\mathrm{R_\odot})^{-1/2}(M/10^6\,\mathrm{M_\odot})^{1/6}$ km s^{-1}, where $\mathrm{M_\odot}$ and $\mathrm{R_\odot}$ are the solar mass and radius, respectively.[1] The other binary member is bound to the MBH. The Galactic Centre hosts a population of young, massive stars which have eccentric, randomly distributed orbits (e.g. Ghez et al. 2008; Gillessen et al. 2009). These S-stars are considered to be the counterparts of the HVSs. There has been significant theoretical work that has gone into modelling the results of binary tidal disruption events (e.g. Gualandris, Portegies Zwart & Sipior 2005; Bromley et al. 2006; Ginsburg & Loeb 2006; Sesana, Haardt & Madau 2007; Antonini et al. 2010; Lu, Zhang & Yu 2010; Sari, Kobayashi & Rossi 2010; Bromley et al. 2012; Kobayashi et al. 2012).

Previous numerical studies by Bromley et al. (2006) have found the disruption probability of a binary at the encounter with an MBH is roughly linear with its penetration depth (the ratio of the closest approach distance to its tidal radius). However, these simulations do not fully explore the deepest penetrations and utilize a full three-body model which is relatively computationally expensive, limiting

★ E-mail: H.M.Brown@2011.ljmu.ac.uk

[1] Velocities in the Galactic halo are lower due to the Galactic potential.

the parameter space that one would be able to reasonably explore. In order to efficiently explore the parameter space, a restricted three-body approximation was proposed (Sari et al. 2010; Kobayashi et al. 2012), and it has been shown that the approximation is very accurate when the binary-to-BH mass ratio is large $M/m \gg 1$. In this method, the essential system parameters are only the binary orientation, the binary phase and the penetration depth, and we can obtain analytic solutions when binaries deeply penetrate the BH tidal radius. This method has also been used to model the velocity distribution of HVSs (Rossi, Kobayashi & Sari 2014), and to fit for the first time current data to given a constrain on the binary properties and the Galactic Potential (Rossi et al. 2017).

All work done utilizing this method has so far only examined circular binaries that are co-planar with their orbit around an MBH. In this paper, we will apply the method to non-coplanar binaries, and we examine how the binary orientation affects the disruption probability and ejection velocities. In Section 2, we describe the restricted three-body approximation, and we discuss how symmetry in the system can be used to further reduce the volume of the parameter space. In Section 3, we numerical obtain the disruption rate of binaries and the energy gain at the BH encounter, and we compare with previous theoretical models. We also discuss the fate of coplanar, eccentric binaries. The conclusions and the implications of our results are discussed in Section 4.

2 PARABOLIC AND RADIAL RESTRICTED THREE-BODY APPROXIMATIONS

In order to discuss the tidal encounter of binaries with an MBH, we employ the restricted three-body approximation presented by Sari et al. (2010), which is valid when the binary mass is much smaller than that of the MBH. In the following discussion, we assume that the masses of the two binary members, the primary m_1 and the secondary m_2 (the total mass $m = m_1 + m_2$), are of the order of solar mass, and the MBH mass M is similar to that of the MBH at the Galactic Centre. Although the exact values of the masses are not important in our formulation, the large mass ratio $M/m \gg 1$ ensures our approximation.

In this approximation, the relative motion of the two binary members $\boldsymbol{r} = \boldsymbol{r}_2 - \boldsymbol{r}_1$ can be formulated as the motion of a single particle under the influence of external time-dependent forces. We apply this approximation to a binary system injected in a parabolic orbit $\boldsymbol{r}_m$ with periapsis r_p around an MBH. Rescaling the distance between the binary members by $(m/M)^{1/3} r_p$ and the time by $\sqrt{r_p^3/GM}$, the equation of motion is given in terms of the dimensionless variables $\boldsymbol{\eta} \equiv (M/m)^{1/3}(\boldsymbol{r}/r_\mathrm{p})$ and t as

$$\ddot{\boldsymbol{\eta}} = \left(\frac{r_p}{r_\mathrm{m}}\right)^3 [-\boldsymbol{\eta} + 3(\boldsymbol{\eta}\cdot\hat{\boldsymbol{r}}_\mathrm{m})\hat{\boldsymbol{r}}_\mathrm{m}] - \frac{\boldsymbol{\eta}}{|\boldsymbol{\eta}|^3}, \tag{1}$$

where $\hat{\boldsymbol{r}}_\mathrm{m} = \boldsymbol{r}_m/r_m = (\cos f, \sin f, 0)$ is a unit vector pointing the centre of mass of the binary, the distance from the MBH is given by $r_\mathrm{m} = 2r_\mathrm{p}/(1+\cos f)$, and f is the angle from the point of closest approach. The angle f, known as the true anomaly, is a function of time, but analytically one has only the time as a function of f. For numerical applications it is preferable to use its differential (and dimensionless) form $\dot{f} = \sqrt{2}(1+\cos f)^2/4$. In Section 3, we will numerically integrate equation (1) and this $\dot{f}$ equation together. We start at a radius well outside the tidal sphere $r_m \gg r_t$, and we evaluate the entire evolution of the binary system by using these equations.

If a binary is ejected towards an MBH around the radius of influence of the BH, the orbital energy is negligible compared to the energy gain or loss of each binary member at the BH encounter. As we have shown, parabolic orbits can be used for the binary's centre of mass to evaluate the characteristic of HVSs (Kobayashi et al. 2012). Since the self-gravity energy of the binary is smaller by a factor of $(M/m)^{1/3} \gg 1$ than the energy gain or loss at the BH encounter, it can also be neglected. This means that the total energy of the system is zero, and the energies of the primary and secondary members are related as $E_1 = -E_2$. In terms of our dimensionless Cartesian coordinates $\boldsymbol{\eta} = (x, y, z)$, the energy is given (Sari et al. 2010; Kobayashi et al. 2012) by

$$E_2 = \frac{Gm_1m_2}{a\,D}\left(\frac{M}{m}\right)^{1/3}\left[\frac{(1+\cos f)^2}{4}(x\cos f + y\sin f) + \frac{-\sin f\,\dot{x} + (1+\cos f)\dot{y}}{\sqrt{2}}\right], \tag{2}$$

where $D = r_p/r_t$ is the penetration factor and r_t is the tidal radius. D indicates how deeply the binary penetrates into the tidal sphere. If the binary dissolves at the BH encounter, this energy becomes a constant, since each binary member is eventually moving only under the conservative force of the BH.

The angular momentum of each binary member around the MBH, $\boldsymbol{L}_i = m_i(\boldsymbol{r}_i \times \dot{\boldsymbol{r}}_i)$ (i=1 or 2), also becomes a constant of the motion when the binary is disrupted. Considering that the positions of the members can be expressed by using the centre of mass $\boldsymbol{r}_m$ and the displacement vector $\boldsymbol{r}$ as $\boldsymbol{r}_1 = \boldsymbol{r}_m - (m_2/m)\boldsymbol{r}$ and $\boldsymbol{r}_2 = \boldsymbol{r}_m + (m_1/m)\boldsymbol{r}$, we can rewrite the angular momenta up to the linear order of r as

$$\boldsymbol{L}_i = \left(\frac{m_i}{m}\right)\boldsymbol{L}_m + \Delta\boldsymbol{L}_i, \tag{3}$$

where $\boldsymbol{L}_m$ is the angular momentum of the centre of mass and $\Delta\boldsymbol{L}_i$ is the angular momentum change of the members at the tidal encounter,

$$\boldsymbol{L}_m \equiv m(\boldsymbol{r}_m \times \dot{\boldsymbol{r}}_m) = \left(0, 0, \sqrt{2GMm^2r_p}\right), \tag{4}$$

$$\Delta\boldsymbol{L}_2 = -\Delta\boldsymbol{L}_1 \equiv \left(\frac{m_1m_2}{m}\right)[\boldsymbol{r}_m \times \dot{\boldsymbol{r}} + \boldsymbol{r} \times \dot{\boldsymbol{r}}_m]. \tag{5}$$

$\Delta\boldsymbol{L}_i$ become constant vectors when the binary is disrupted. The exact values can be estimated by using equation (1) in a similar way as we have evaluated E_i. However, considering $r_m \sim r_t$ and $|\dot{\boldsymbol{r}}_m| \sim \sqrt{GM/r_t}$ at the binary disruption, $|\Delta\boldsymbol{L}_i|$ is about $(M/m)^{1/3}\sqrt{Gm^3a}$. This is smaller by a factor of $\sim D^{1/2}(M/m)^{1/3} \gg 1$ than L_m. The angular momentum change at the tidal encounter is not important if it is not a very deep encounter.

After the tidal disruption, the eccentricities of their orbits around the MBH are given by $e_i = \sqrt{1 + 2L_i^2E_i/m_i^3G^2M^2}$. If $E_i < 0$ ($E_i > 0$), the member is captured (ejected). For $D \gg (m/M)^{2/3}$, we can neglect the linear terms $\Delta\boldsymbol{L}_i$ in their angular momenta, and we obtain the eccentricity of the captured member as

$$1 - e_i \sim 2D\left(\frac{m_1m_2}{m_im}\right)\left(\frac{m}{M}\right)^{1/3}|\bar{E}|. \tag{6}$$

where $\bar{E}$ is the energy gain E_2 in units of $(Gm_1m_2/a)(M/m)^{1/3}$. Since $|\bar{E}|$ is expected to be of order of unity, the bound orbit would be very eccentric (Hills 1991; Pfahl 2005; Kobayashi et al. 2012).

Since in this framework, results can be simply rescaled in terms of binary masses, their initial separation, and the binary-to-BH mass ratio, the system is essentially characterized by four parameters for circular binaries: the penetration factor D, the initial binary phase

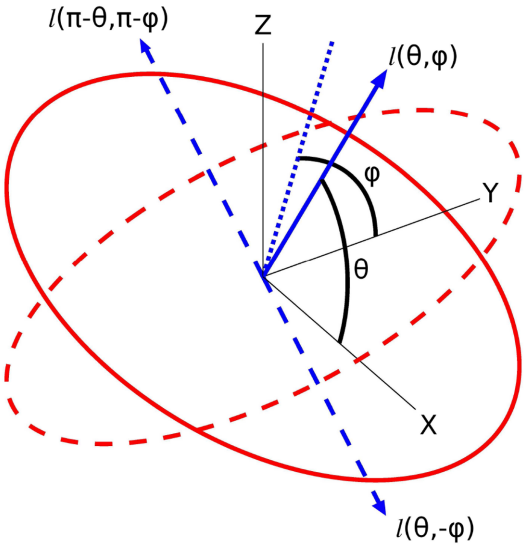

Figure 1. The initial circular orbit of a binary (red solid line) and its angular momentum vector (blue solid arrow) with its projection (blue dotted line) on the *Y*–*Z* plane. The binary itself orbits the MBH on a parabolic orbit on the *X*–*Y* plane. The red dashed line indicates another circular orbit which is symmetric to the red solid orbit with respect to the *X*–*Y* plane. The two blue dashed arrows are the angular momenta of the same (red dashed) orbit but orbiting in the opposite direction.

ϕ, and the orientation (θ, φ) of the binary's angular momentum, where θ is the inclination angle measured from the positive x-axis and φ is the azimuth angle measured from the positive y-axis on the y–z plane (see the blue solid arrow in Fig. 1). For eccentric binaries, we have two additional parameters: the eccentricity e of the orbits and the direction of the semimajor axis. We characterize the latter by the vector connecting the binary's centre of mass to the secondary member's periapsis. Although our formalism can be applied to explore the fate of a binary with an arbitrary orbit orientation, we will discuss only coplanar binaries when we numerically study the evolution of eccentric binaries in the next section. The direction of the vector (i.e. the direction of the semimajor axis) will be given by an angle ϖ measured from the positive x-axis.

By considering two kinds of pairing of solutions which originate from symmetry in the system, we can further reduce the volume of the parameter space.

(i) The negative of a solution is also a solution for equation (1). However, since the energy equation (2) is also linear in the coordinates, for circular binaries, a body starting with a phase difference π will have the same final energy in absolute value but the opposite in sign (Sari et al. 2010). The ejected (captured) member is captured (ejected) if the initial binary phase is increased by π. We just need to sample the binary phase ϕ between 0 and π. For eccentric binaries, this is translated to the orientation of the semimajor axis and ϖ should be sampled between 0 and π (the binary phase ϕ should be considered between 0 and 2π). For non-coplanar eccentric binaries, ϖ should be redefined appropriately (e.g. if the direction vector of the semimajor axis is projected in the x–y plane, we would use the angle between the projected vector and x-axis), but we still need to sample it only between 0 and π.

(ii) Another kind of pairing is possible if one notices that the system is symmetric with respect to the x–y plane. If $\{x(t), y(t), z(t)\}$ is a solution, $\{x(t), y(t), -z(t)\}$ is also a solution (see the red solid and dashed lines in Fig. 1). Since the energy equation (2) does not depend on $z(t)$, they have the same energy as expected. If the orientation of a binary is parametrized by (θ, φ) as $\hat{l} = (\cos\theta, \sin\theta\cos\varphi, \sin\theta\sin\varphi)$, a sphere is defined by $\hat{l}$ for generic (θ, φ). One might think at first that there is correspondence between points on the sphere which are located symmetrically with respects to the x–y plane: $(\theta, \varphi) \leftrightarrow (\theta, -\varphi)$. However, the binaries should rotate in the same direction when they are projected in the x–y plane. The correspondence actually exists between points symmetric about z-axis: $(\theta, \varphi) \leftrightarrow (\pi - \theta, \pi - \varphi)$. Note that $(\theta, -\varphi)$ and $(\pi - \theta, \pi - \varphi)$ indicate the same binary orientation except the rotation direction (i.e. clockwise or anticlockwise). To investigate how the orientation of circular or eccentric binaries affects the disruption process, it is sufficient if we consider only the hemisphere defined by $0 \leq \theta \leq \pi/2$ and $0 \leq \phi < 2\pi$ (i.e. the fore-side of the sphere).

2.1 Radial approximation

In the limit of deep penetrations $D \ll 1$, the trajectory of the binary's centre of mass becomes almost radial. By assuming a radial orbit for the trajectory, we can obtain another set of approximation formulae. This radial approximation is useful when we investigate the binary disruption process in the deep penetration limit. Since the binary orientation is determined by a single parameter (i.e. the angle between the binary rotation axis and the radial direction), the discussion is simpler. However, the difficulty arises from the assumption of a purely radial orbit with which the binary goes straight towards the BH. A deep parabolic orbit with $D \ll 1$ parallels closely the radial one and gets around the BH smoothly. Since the energy gained by one of the binary members (or the energy loss by the other) during the periapsis passage is smaller by a factor of $D^2 \ll 1$ than gained (or lost) around the tidal radius, the perturbations caused by the binary mutual gravity is negligible around the passage, each of the binary members turns around with a constant orbital energy [see Sari et al. (2010) for the details]. Therefore, we can connect an incoming radial orbit with an outgoing radial one. For this purpose, we use free solutions which are available when the binary is well within the tidal radius. Since around the periapsis passage ($t = 0$), the BH tides dominate over the mutual gravity of the binary, the last term in the right-hand side of equation (1) is negligible. When the centre of mass of the binary moves on a radial orbit, the relative position of the binary members $\boldsymbol{r} = \boldsymbol{r}_2 - \boldsymbol{r}_1$ are given by (Sari et al. 2010),

$$\begin{aligned} x(t) &= A_x|t|^{-1/3} + B_x|t|^{4/3}, \\ y(t) &= A_y|t|^{1/3} + B_y|t|^{2/3}, \\ z(t) &= A_z|t|^{1/3} + B_z|t|^{2/3}, \end{aligned} \tag{7}$$

where the distances and the time have been scaled by the initial semimajor axis of the binary a and the inverse angular frequency of the binary $\sqrt{Gm/a^3}$, respectively. We can ferry the free solution across $t = 0$, from negative to positive times by simply changing the sign of the A coefficients. More specifically, we evaluate the six coefficients by using the numerical position (x, y, z) and velocity (v_x, v_y, v_z) at $t = -t_{\rm min} < 0$. Then, we resume the radial three-body approximation calculations at $t = t_{\rm min} > 0$. We have evaluated the evolution of the system based on the radial approximation with different values of $t_{\rm min}$, and we find that the difference in the ejection energy becomes less than 0.1 per cent for $t_{\rm min} < 10^{-6}$. We will use $t_{\rm min} = 10^{-6}$ for radial approximation calculations.

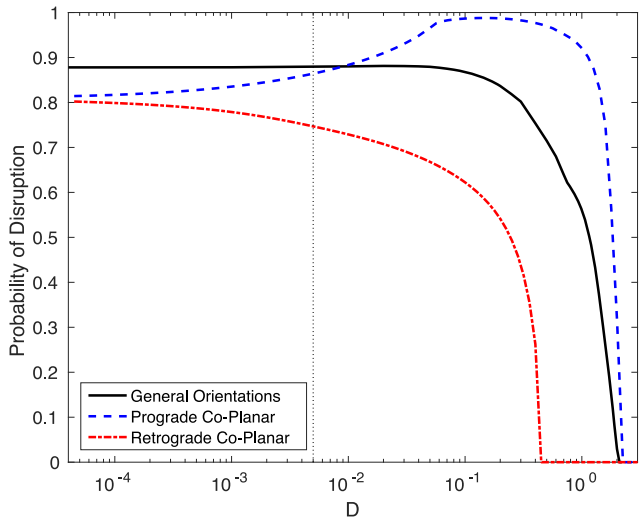

Figure 2. Probability of disruption as a function of the penetration factor D. General binary orientations (black solid), coplanar prograde orbits (blue dashed), and coplanar retrograde orbits (red dot–dashed). The vertical dotted line marks the penetration limit for binaries of solar-type stars with a= 1 au, where the individual stars undergo tidal disruption.

3 NUMERICAL RESULTS

3.1 Circular binaries

Our numerical calculations utilize a fourth-order Runge–Kutta method to integrate the equations of motion. The time steps of the integration are scaled by the minimum value of the three dynamical times associated with the binary pair and the interaction between each binary member and the BH. Circular binaries are injected in parabolic orbits around an MBH. To uniformly sample the binary orientation, we populate the surface of a unit sphere with equally spaced 2000 grid points. The regular equidistribution can be achieved by choosing circles of latitude at constant intervals d_θ and on these circles points with distance $d_\varphi \sim d_\theta$. For each grid point, the binary phase ϕ is sampled with 200 equally spaced grid points between 0 and π.

Fig. 2 indicates the probability of binary disruption at the BH encounter as a function of D averaged over phase and orientation. The largest D for which there is disruption is D= 2.1 for the coplanar prograde orbits and for all sampled orbits. This indicates that coplanar prograde orbits have the highest disruption chance for the shallow encounters. For shallow penetrators $D \sim$ 1–2, the disruption probability is approximately linear with D. Bromley et al. (2006) have reported a linear relationship $P_{\rm dis} \sim 1 - D/2.2$. However, for smaller D, the disruption rate plateaus with ∼88 per cent (the black solid line). Interestingly, about 12 per cent of binaries survive the BH encounter even for very deep penetrators $D \ll 1$. Our numerical results can be well approximated by a fifth-order polynomial,

$$P_{\rm dis}(D) = A_0 + A_1 D + A_2 D^2 + A_3 D^3 + A_4 D^4 + A_5 D^5, \qquad (8)$$

with coefficients: $A_0 = 0.8830$, $A_1 = -0.0809$, $A_2 = -1.0541$, $A_3 = 1.5377$, $A_4 = -0.9249$, $A_5 = 0.1881$ for $D < 2.1$. The fractional error $\Delta P_{\rm dis}/P_{\rm dis}$ is less than 1 per cent for $D \lesssim 1$. As the disruption probability approaches zero around $D \sim 2$, the fractional error becomes larger, but it is still about 5 per cent at $D = 1.8$ and about 20 per cent at $D = 2$. This disruption rate 88 per cent at $D \ll 1$ is higher than that for coplanar binaries. Both coplanar prograde (the blue dot–dashed line) and retrograde (the red dot–dashed line) cases saturate at a level of ∼80 per cent (Sari et al. 2010).

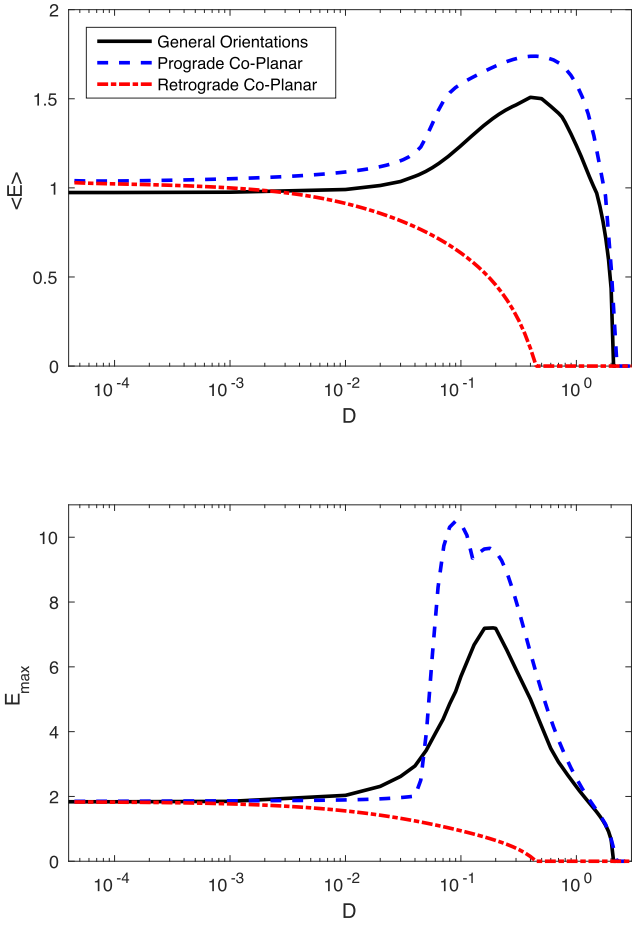

Figure 3. Top panel: Ejection energy averaged over binary phase and orientation as a function of D. Bottom panel: Characteristic maximum ejection energy as a function of D. For a given D, the top 1 per cent have ejection energy higher than the characteristic maximum energy $E_{\rm max}$. General binary orientations (black solid), coplanar prograde orbits (blue dashed), and coplanar retrograde orbits (red dot–dashed). The average and characteristic maximum energy are in units of $(Gm_1m_2/a)(M/m)^{1/3}$, and they are evaluated for the absolute value of the energy $|E|$.

The disruption rate estimates for $D \ll 1$ break down when the pericentre distance to the MBH becomes comparable to the tidal disruption radius of the binary members (i.e. individual stars). If the binary members are solar-type stars with radius $\rm R_\odot$ and its initial separation is a = 1 au, the stars themselves are disrupted for $D \lesssim \rm R_\odot/\mathit{a} \sim 5 \times 10^{-3}$ (the vertical dotted line in Fig. 2). To achieve a smaller D, the initial separation a should be wider, or the binary members should be compact objects such as stellar mass BHs, neutron stars and white dwarfs. The evolution of a stellar mass BH binary should be well described by the point-particle model. However, if the periapsis is close to the event horizon scale R_g of the central MBH, the Newtonian formulation would break down. Relativistic effects are negligible for $D \gg (m/M)^{1/3} R_g/a \sim 8 \times 10^{-4} (a/1\,{\rm au})^{-1} (m/4\,{\rm M_\odot})^{1/3} (M/4 \times 10^6\,{\rm M_\odot})^{2/3}$.

The top panel of Fig. 3 shows the ejection energy averaged over the binary phase and orientation as a function of D. We also plot in the bottom panel the characteristic maximum ejection energy $E_{\rm max}$ for a given D as a function of D. This is estimated to characterize

the population of the highest energy gain cases, the top 1 per cent of the sampled cases have ejection energy higher than this energy. This threshold value is rather insensitive to the grid resolution, compared to the actual maximum value which is as high as ∼27 for a coplanar prograde orbit with $D \sim 0.1$. In both plots, a peak is present (the black solid lines), and the peak values are lower than for the prograde orbits (the blue dot–dashed lines). There are two peaks in the $E_{\rm max}$ distribution for the prograde orbits. The average energy is approximated by a polynomial,

$$\langle E \rangle = A_0 + A_1 D + A_2 D^2 + A_3 D^3 + A_4 D^4 + A_5 D^5, \quad (9)$$

with coefficients: $A_0 = 0.9582$, $A_1 = 3.3268$, $A_2 = -6.6801$, $A_3 = 5.2785$, $A_4 = -1.8731$, $A_5 = 0.2260$, where this energy is in units of $(Gm_1m_2/a)(M/m)^{1/3}$. The fractional error is less than 1 per cent for $D \lesssim 1$, and it is about 3 per cent at $D = 1.8$ and about 10 per cent at $D = 2$. By equalizing this energy in the physical units with the kinetic energy $m_1 v_1^2/2$ (or $m_2 v_2^2/2$), we can estimate the ejection velocity of the primary (or secondary) star at a distant place from the BH. The Galactic potential should be taken into account separately to estimate the velocity in the halo (e.g. Rossi et al. 2014, 2017).

The eccentricities of bound stars are given by $1 - e \sim D(m/M)^{1/3}|\bar{E}|$ for equal mass binaries. Assuming $M/m = 10^6$, the mean eccentricity difference $1 - \langle e \rangle$ and the characteristic maximum difference $1 - e_{\rm min}$ are shown as a function of D in Fig. 4. If we consider deep penetrators, since $\langle \bar{E} \rangle \sim 1$ and $E_{\rm max} \sim 2$ for $D \ll 1$ (see Fig. 3), the mean value is given by $1 - \langle e \rangle \sim 10^{-2} D$ and $1 - e_{\rm min}$ is larger by a factor of ∼2. For very deep penetrators $D \lesssim (m/M)^{2/3} = 10^{-4}$, the distributions flatten out even in a log-log plot as $\Delta \boldsymbol{L}_i$ contributes to $\boldsymbol{L}_i$ (since the behaviour around $D \sim 1$ is more important in the context of HVS study, $1 - e$ is plotted in the linear scale). Shallow penetrators $D \sim 1$ give lower eccentricities, but they are still very high $e \sim 0.98$–0.99 (Miller et al. 2005; Perets, Hopman & Alexander 2007) for S-stars in the Galactic Centre ($0.3 \lesssim e \lesssim 0.95$; Ghez et al. 2008; Gillessen et al. 2009), suggesting that post-capture relaxation is the significant factor in determining S-star eccentricities (Perets et al. 2009; Alexander 2017).

We also investigate how the disruption probability depends on the inclination angle θ. As we have discussed in the previous section, since there is correspondence between (θ, φ) and $(\pi - \theta, \pi - \varphi)$, the disruption probability (and the energy averaged over binary phase) should be the same for the two binary orientations: $P_{\rm dis}(\theta, \varphi) = P_{\rm dis}(\pi - \theta, \pi - \varphi)$. By integrating this relation with respect to φ, we obtain the symmetry about $\theta = \pi/2$: $P_{\rm dis}(\theta) = P_{\rm dis}(\pi - \theta)$. The numerical disruption probability is shown in Fig. 5 as a function of θ for a fixed D. We can clearly see such symmetry about $\theta = \pi/2$.

For deep penetrators $D \ll 1$, where the trajectory of the binary's centre of mass becomes radial, the binary orientation should be characterized only by the inclination angle θ (i.e. the angle between the radial direction and the binary rotation axis). Prograde or retrograde has no meaning or influence in this limit; indeed in Fig. 2, prograde and retrograde results overlap in this regime. The radial approximation (the blue circles in the upper panel of Fig. 5) is in a good agreement with the very deep penetrations ($D = 10^{-5}$, the blue solid line) and the fractional difference in the probability of disruption between the radial and parabolic approximations becomes less than 2 per cent for $D < 10^{-4}$. Almost all binaries will be disrupted when the binary rotation axis is roughly oriented towards the BH or it is in the opposite direction. However, the surviving probability becomes significant for $0.15\pi \lesssim \theta \lesssim 0.85\pi$, the highest surviving probability (or the lowest disruption probability ∼80 per cent) is achieved for

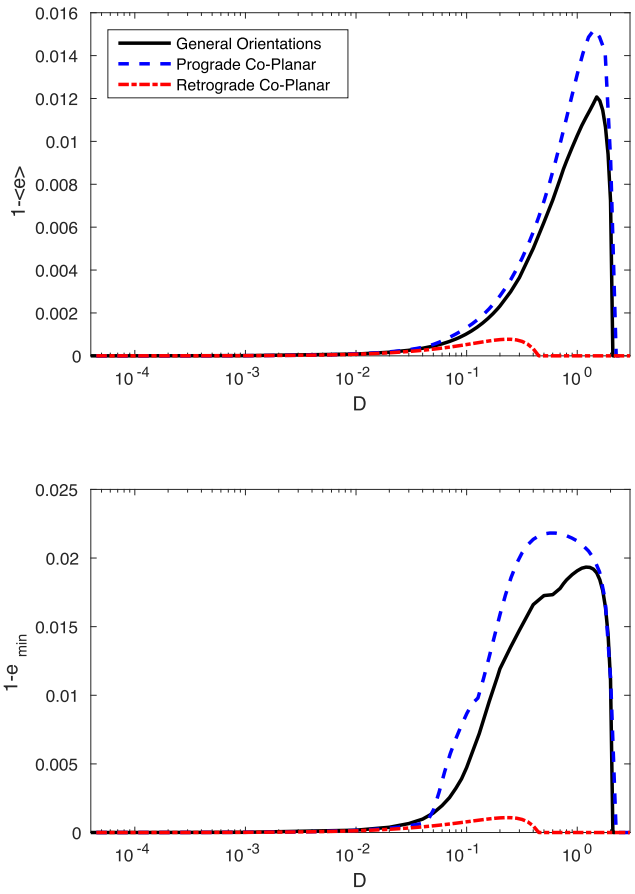

Figure 4. Top panel: Mean eccentricity difference from a parabolic orbit in bound stars as a function of D. Bottom panel: Maximum eccentricity difference from a parabolic orbit in bound stars as a function of D, the bottom 1 per cent have eccentricity lower than the characteristic minimum eccentricity $e_{\rm min}$. General binary orientation (black solid), coplanar prograde orbits (blue dashed), and coplanar retrograde orbits (red dot–dashed). $m_1 = m_2$ and $M/m = 10^6$ are assumed.

$\theta = \pi/2$. For larger values of D, the surviving probability increases for values of θ closer to 0 and π.

For very shallow penetrators, the highest disruption probability is archived around $\theta = \pi/2$, rather than $\theta \sim 0$ or π (see the black dotted line in the bottom panel). This is because the dynamics depends on the relative orientation of the binary and orbital angular momenta for shallow penetrators, coplanar prograde orbits are relatively vulnerable to disruption.

Fig. 6 indicates the ejection energy averaged over binary phase and the azimuth angle for a given D as a function of the inclination angle θ. As we have discussed, the average energy is symmetric about $\theta = \pi/2$, the numerical results are plotted for $0 < \theta < \pi/2$. The radial approximation results (the blue circles) and the parabolic approximation results for $D = 10^{-5}$ (the blue solid line) are almost identical in this figure. However, there is a discrepancy at $\theta = 0$. Due to the nature of the radial approximation binaries with $\theta = 0$ have zero energy at all times. The parabolic approximation gives non-zero energy and its energy distribution is smooth around $\theta = 0$. For a wide range of D, the average energy slightly increases as the inclination angle θ increases. For the parabolic approximation results, the energy for $\theta = \pi/2$ is higher by a factor of 1.4–1.7 than that for $\theta = 0$. Since the eccentricity differences $1 - e$ of bound orbits are proportional to their orbital energy, the bound

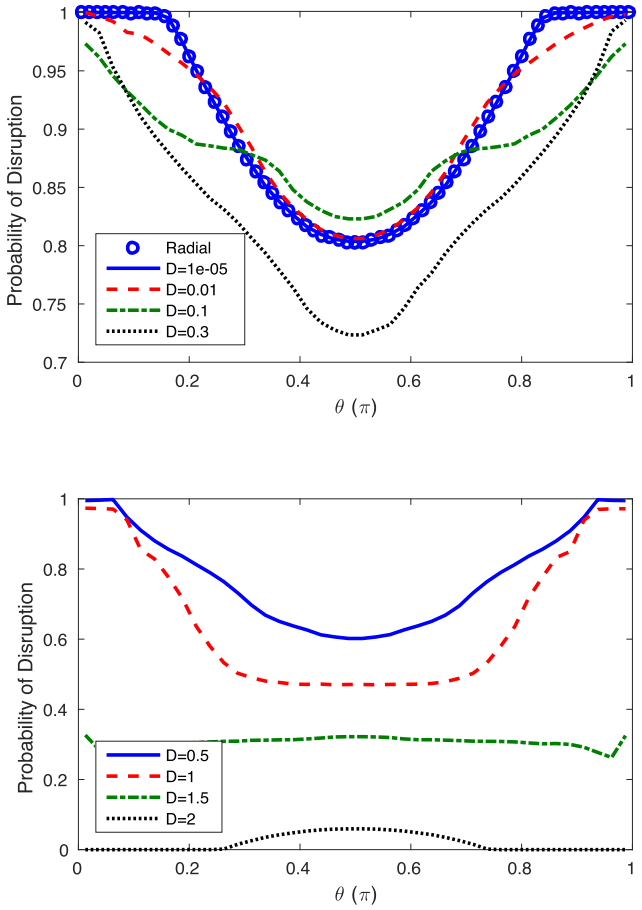

Figure 5. Probability of disruption for a given D as a function of the inclination angle θ. Upper panel: deeper penetrators: the radial approximation (blue circles) and the parabolic approximation with $D = 10^{-5}$ (blue solid), 10^{-2} (red dashed), 10^{-1} (green dot–dashed), and 0.3 (black dotted). Bottom panel: shallower penetrators: the parabolic approximation with D= 0.5 (blue solid), 1.0 (red dashed), 1.5 (green dot–dashed), and 2.0 (black dotted).

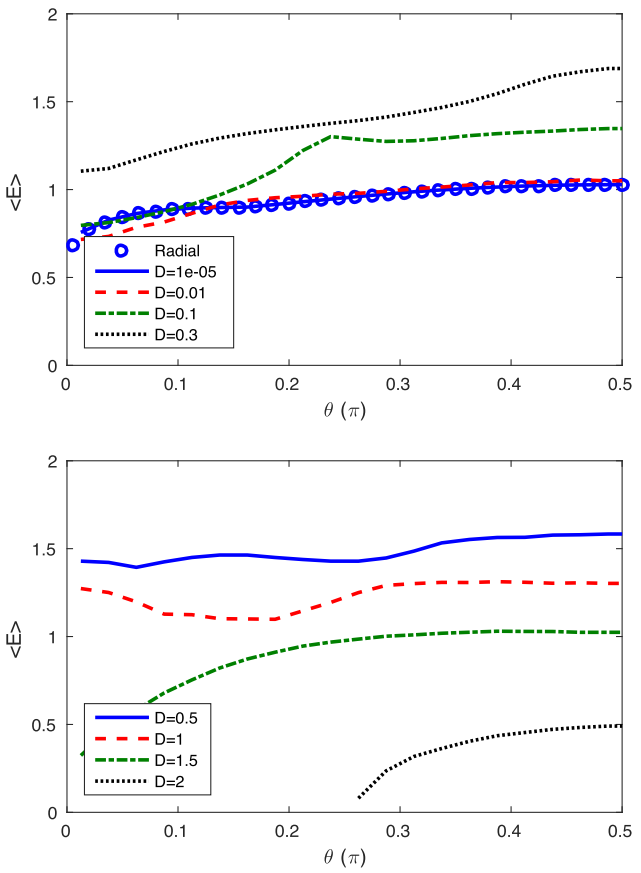

Figure 6. Ejection energy averaged over binary phase and azimuth angel for a given D as a function of the inclination angle θ. Radial solution (blue crosses) and parabolic solutions with $D = 10^{-5}$ (blue solid line), $D = 10^{-2}$ (red dashed line), $D = 0.1$ (green dot–dashed line), $D = 0.3$ (black dotted line). The average energy is in units of $(Gm_1m_2/a)(M/m)^{1/3}$, and it is evaluated for the absolute value of the energy $|E|$.

orbits are slightly less eccentric for $\theta = \pi/2$. However, as we have discussed, the eccentricities of the S-stars are determined by post-capture relaxation processes.

3.2 Deep encounter survivors

The existence of surviving binaries for $D \ll 1$ was first discussed by our group (Sari et al. 2010). Recently, Addison, Laguna & Larson (2015) also reported a population of such surviving binaries in their large Monte Carlo simulations. Although deep encounter survivors are counter-intuitive, all binaries including these peculiar ones are actually disrupted when deeply penetrating the tidal sphere, and the binary members separate. However, they approach each other after the periapsis passage and a small fraction of them can form binaries again.

To discuss this behaviour in more detail, we consider the radial restricted three-body approximation. Since the binary orientation is described by a single parameter in this regime, the discussion is simpler. As we have discussed in Section 2.1, we have analytic solutions equation (7) when the binary deeply penetrates the tidal sphere. Since we have a set of three linear differential equations of the second order, all solutions are linear combination of six independent solutions. Each could be physically obtained by taking the difference between an orbit infinitesimally close to a radial orbit and the radial orbit itself. In equation (7), the A_x solution describes two particles that have the same trajectory, but are slightly separated in time. The B_x solution describes the relative orbits of two particles going on the same radial path, but with slightly different energies. The energy gain or loss at the tidal encounter is proportional to B_x [see Sari et al. (2010) for the full discussion].

From equation (7), we can see that the A_x solution dominates as the binary approach the 'periapsis' ($t = 0$; note that the radial approximation corresponds to the parabolic approximation in the deep penetration limit). In other words, the binary members are always in the same radial trajectory in the final approach stage, but they are separated in time. As the binary deeply penetrates the tidal sphere, the binary members separate wider and wider in the radial direction. However, they always approach each other after the periapsis passage $x \sim A_x|t|^{-1/3}$.

Although they approach each other, since the other free solutions begin to grow at $t > 0$ (the index of the B_x solution is the largest), they separate again in most cases. Only a small fraction of the pairs come out the tidal sphere as a binary. Although we do not fully understand the condition which ensures the binary formation after the periapsis passage, we have interesting results which indicate that the A_x and B_x solutions are likely to be related to the process.

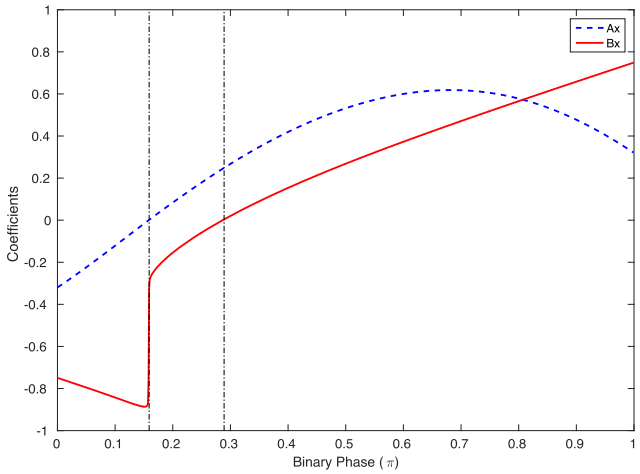

Figure 7. The coefficients of the free solutions as functions of the initial binary phase: A_x (blue dashed) and B_x (red solid). the binary inclination $\theta = 0.3\pi$. Binaries survive the deep tidal encounter if the initial binary phase is in a narrow range indicated by the vertical black dot–dashed lines.

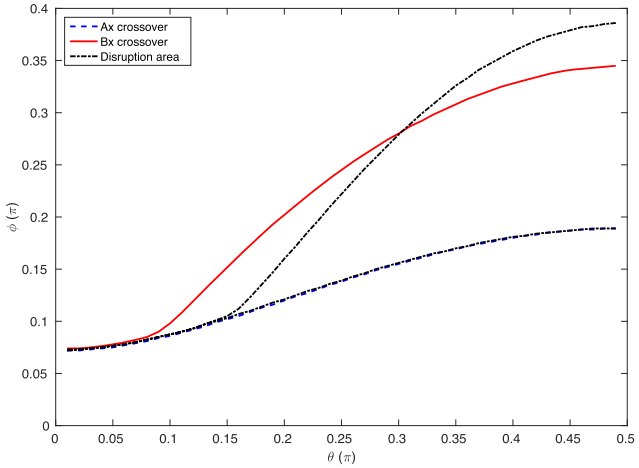

Figure 8. The positions in the parameter space for which the coefficients of the free solution A_x (blue dashed) and B_x (red solid) are equal to zero and the boundaries of the range of binary phase for which binaries survive the deep tidal encounter (black dot–dashed).

Fig. 7 shows the range of the initial binary phase ϕ for which binaries survive the deep encounter (i.e. binary formation after the periapsis passage). This is obtained based on the radial restricted three-body approximation with the binary inclination angle $\theta = 0.3\pi$. The coefficients A_x (the blue dashed line) and B_x (the red solid line) are also shown as functions of ϕ. These coefficients are evaluated at $t = -t_{\rm min} = -10^{-6}$, and they are expected to become constants if the binary is disrupted (and the members separate widely). We notice interesting behaviours of the lines at the boundaries of the surviving region (the vertical dot–dashed lines). A_x becomes zero and the value of B_x jumps at the left boundary, and B_x is close to zero at the right boundary. The energy gain/loss of the binary members is proportional to B_x, large energy gain/loss near the surviving region has been reported in the previous study (e.g. fig. 6 in Sari et al. 2010). Although we have plotted the surviving range and the coefficients for $0 < \phi < \pi$, a binary starting with a phase difference π will have the same results (i.e. disrupted or not) and the same coefficients in absolute values but the opposite in sign.

Fig. 8 shows how the boundaries of the surviving region (the black dot–dashed lines) and the initial binary phases at which $A_x = 0$ (the blue solid line) or $B_x = 0$ (the red solid line) depend on the binary inclination angle θ. At a large inclination angle (e.g. $\theta = \pi/2$), binaries survive the tidal encounter for a wide range of ϕ. As a smaller inclination angle is assumed, the surviving region becomes narrower, and there are practically no survivors for $\theta < 0.15\pi$ (or $\theta > 0.85\pi$). In the figure, the $A_x = 0$ line is identical to one of the boundaries of the surviving region (the lower branch). If A_x is zero, the binary is just tidally compressed (i.e. no tidal stretch) when it approach the periapsis. Although the $B_x = 0$ (or equivalently $E = 0$) line is similar to the other boundary (the upper branch) of the surviving region, they are slightly different. We notice that the value of B_x slightly evolve even at $t > 0$ around the boundary, because the binary members do not separate quickly in this region and they weakly interact each other. The real $E = 0$ line is expected to be identical to the upper branch of the boundaries or slightly inside the surviving region. Otherwise, it means that some binaries are disrupted even if the energy gain or loss at the tidal encounter is zero ($E = 0$). If the binary inclination angle θ is 0 or π (i.e. the binary rotation axis is exactly oriented towards the BH or it is in the opposite direction), from the symmetry of the system, the three-body interaction does not depend on the binary phase ϕ and we obtain $A_x = B_x = 0$ for any ϕ.

As we have just shown, for a given penetration depth and binary orientation, the fate of binaries (disrupted or not) is determined by the initial binary phase ϕ. If ϕ is in a narrow surviving region, the binary survives the tidal encounter. It means that we can determine the probability of disruption accurately by resolving the narrow region with high-resolution grid points. The advantage of our method is that we can analytically handle some of the system parameters (e.g. masses of the binary members, initial binary separation, binary-to-BH mass ratio). The number of essential parameters is smaller than that for the full three-body calculations. This allows us to set up high-resolution grid points in the parameter space, rather than doing random sampling in the parameter space.

We had checked the numerical convergence of our numerical results. For example, the probability of disruption shown in Fig. 2 (general orientations, the black solid line) is obtained with $N_{\rm ori} = 2000$ equally spaced grid points on a unit sphere (the orientation of a binary) and $N_{\rm pha} = 200$ equally spaced grid points for the binary phase. The results are about 87 per cent for $D = 10^{-3}$ and 10^{-1}. The probability is evaluated by changing $N_{\rm ori}$ or $N_{\rm pha}$ by a factor of 1/4−4. The probability changes less than 0.3 per cent for the lower resolution (a factor of 1/4–1), and less than 0.05 per cent for the higher resolutions (a factor of 1–4).

3.3 Eccentric binaries

We now consider the tidal disruption of coplanar, eccentric binaries. As we have discussed in the previous section, we sample ϖ uniformly between 0 and π. Since eccentric binaries spend a larger fraction of their time near the apoapsis, the binary phase $0 < \phi < 2\pi$ is sampled with unequally spaced grids with which the binary rotates from a grid point to the next one with a constant time step. The time-averaged binary separation is given by $\bar{a} = a(1 + e^2/2)$, where a is the semimajor axis.

The top panel of Fig. 9 shows the disruption probability of eccentric binaries as a function of D. All cases give ∼80 per cent disruption probability for $D \ll 1$. However, for shallow penetrators,

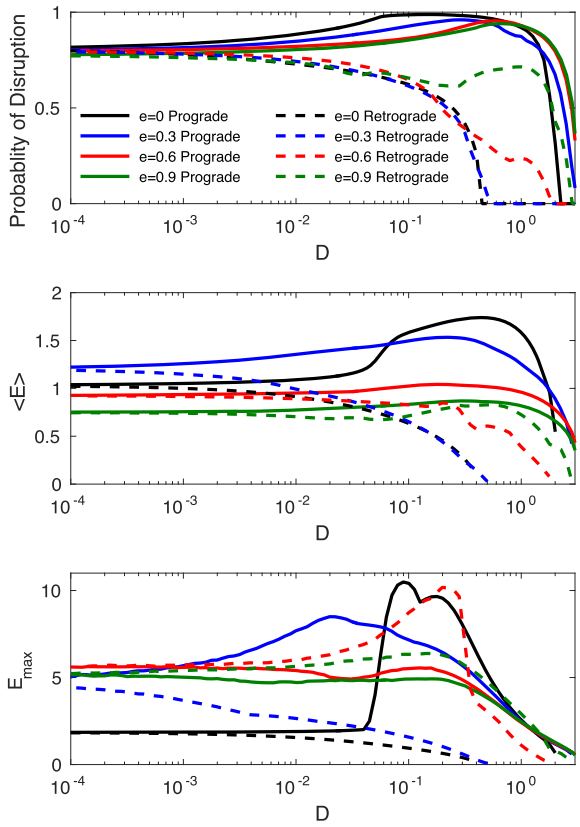

Figure 9. Top panel: Probability of disruption. Middle panel: Ejection energy averaged over binary phase and the orientation of the semimajor axis. Bottom panel: Characteristic maximum ejection energy. These quantities are plotted as a function of the penetration factor D for coplanar prograde (solid) and retrograde (dashed) orbits with $e = 0$, 0.3, 0.6, and 0.9 (black circles, blue crosses, red plusses, and green triangles, respectively). The average and characteristic maximum energy are in units of $(Gm_1m_2/a)(M/m)^{1/3}$, and they are evaluated for the absolute value of the energy $|E|$.

the disruption probability strongly depends on the eccentricity and the direction of the binary rotation. For prograde orbits (the solid lines), as higher eccentricity is assumed, the peak is shifted at a larger D, and the largest penetration factor $D_{\rm max}$ for which there is disruption also becomes larger. $D_{\rm max}$ is $\sim$2.1 for $e = 0$, $\sim$2.8 for $e = 0.3$ and $\sim$3.2 for $e = 0.6$ and 0.9. Since we have defined the penetration factor $D \propto a^{-1}$ by using the semimajor axis a, the effective binary separation $\bar{a}$ is larger than a, and consequently, the effective penetration factor define with $\bar{a}$ is smaller by a factor of $(1 + e^2/2)$ than D. For higher eccentricity, binaries are disrupted at a larger value of D, and the peak is shifted at a larger D. Although this qualitatively explains the shifts, the actually shits are larger (i.e. eccentric binaries are more vulnerable than circular ones at shallow encounter). For retrograde orbits (the dashed lines), the eccentricity more significantly affects the probability distribution at shallow encounter. Although the results for $e = 0$ and 0.3 are similar, the probability distributions for $e = 0.6$ and 0.9 have a peak structure around $D = 1$, and $D_{\rm max}$ is much larger than the circular case ($D = 0.44$ for $e = 0$), they are comparable to the values for the corresponding prograde orbits.

We plot the ejection energy averaged over the binary phase ϕ and orientation ϖ in the middle panel of Fig. 9. We have scaled the energy by using the semimajor axis a as $(Gm_1m_2/a)(M/m)^{1/3}$. For prograde orbits (the solid lines), as higher eccentricity is assumed, the distribution becomes flatter. The peak structure around $D = 0.1-1$ which is significant for circular binaries ($e = 0$; the black solid line) disappears. For retrograde orbits, for higher eccentricity, the distribution extends to larger D because of a larger $D_{\rm max}$, and the distribution becomes similar to the prograde one. In the deep penetration limit $D \ll 1$, the prograde and retrograde orbit cases approach the same ejection energy as expected. Interestingly, the asymptotic energy is not a monotonic function of the eccentricity, the largest value is given by $e = 0.3$ (the blue lines).

The distributions of the characteristic maximum energy $E_{\rm max}$ also behave in a similar way especially for the prograde orbits (the solid lines in the bottom panel): the distributions becomes flatter for higher eccentricity. However, the distributions for retrograde orbits (the dashed lines) have a peak structure for high eccentricity, it is significant especially for $e = 0.6$ (the red dashed line). The values around $D = 0.1$ become even larger than the corresponding prograde cases for $e = 0.6$ and 0.9 (the red and green lines). The asymptotic values at $D \ll 1$ are similar for prograde and retrograde orbits, and higher eccentricity gives a higher value.

The asymptotic values at $D \ll 1$ are also estimated by using the radial approximation. Although the disruption probability at $D \ll 1$ is less sensitive to the eccentricity (see the top panel of Fig. 10), there is a small dip around $e = 0.5$. The average ejection energy has been scaled by $(Gm_1m_2/a)(M/m)^{1/3}$. Since the effective binary separation $\bar{a}$ is larger than the semimajor axis, the disruption of a wider binary should result in an ejection energy smaller by a factor of $(1 + e^2/2)$. The numerical results show a smaller energy for $e = 0.9$, compared to the circular case $e = 0$ (see the middle panel of Fig. 10), and the number is roughly consistent: $1/(1 + e^2/2) \sim 0.7$. However, the numerical energy peaks around $e = 0.35$. The eccentricity more drastically affects $E_{\rm max}$ (see the bottom panel). The values at $e > 0.4$ is much larger than that for the circular case, and there is a significant peak around $e = 0.35$.

4 CONCLUSIONS AND DISCUSSION

We have discussed how binary tidal disruption depends on the inclination and eccentricity of the binary. When the binary-to-BH mass ratio is large $M/m \gg 1$, our restricted three-body approximation allows us to explore the parameter space efficiently. For inclined, circular binaries, we have shown that about 12 per cent of them with random orientations survive even if they approach the massive BH very closely: $D \ll 1$. Although the existence of the surviving binaries is counter-intuitive, the binary members actually once separate even in the surviving cases, and approach each other again after their periapsis passage. This surviving probability is lower than $\sim$20 per cent obtained for coplanar cases (Sari et al. 2010). This is because almost all deep penetrators are disrupted when the binary rotation axis is roughly oriented towards the massive BH or in the opposite direction (i.e. the inclination $\theta \lesssim 0.15\pi$ or $\theta \gtrsim 0.85\pi$). The maximal surviving probability is achieved for $\theta = \pi/2$ for a wide range of D; however, if D is close to the largest D for which there is disruption, disruption is only found in prograde coplanar orientations. The average energy $\langle E \rangle$ also depends on the inclination θ, but the dependence is weak. The energy for $\theta = \pi/2$ is higher by a factor of 1.4$-$1.7 than that for $\theta = 0$.

Our coplanar calculations show that the disruption probability at $D \ll 1$ is insensitive to the eccentricity of binaries, all cases of prograde and retrograde orbits with $e = 0-0.9$ give very similar disruption probability. The ejection energy at $D \ll 1$ is more sensitive to the eccentricity. This can be partially explained by an effectively

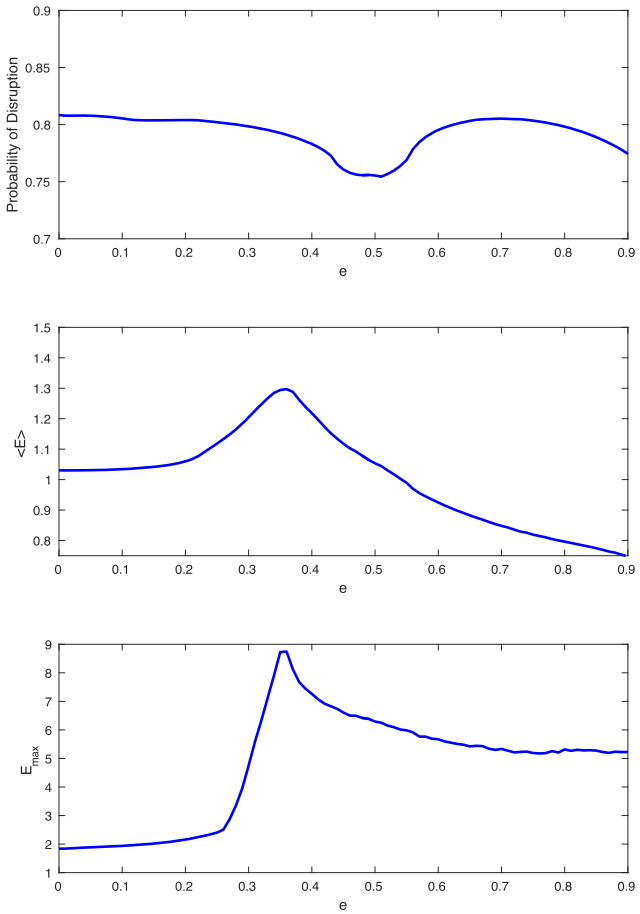

Figure 10. Radial approximation results for the inclination angle $\theta = \pi/2$. Top panel: Probability of disruption as a function of eccentricity. Middle panel: Ejection energy averaged over binary phase and the direction of the semimajor axis as a function of eccentricity. Bottom panel: Characteristic maximum ejection energy as a function of eccentricity. The average and characteristic maximum energy are in units of $(Gm_1m_2/a)(M/m)^{1/3}$, and they are evaluated for the absolute value of the energy $|E|$.

wider binary separation for more eccentric binaries. However, the energy is not a monotonic function of the eccentricity, and it peaks at $e \sim 0.35$. For shallow penetrators, both disruption probability and ejection energy are more strongly affected by the eccentricity, especially in retrograde orbits where disruption rates become closer to that of prograde orbits with higher eccentricity.

Our results were obtained assuming point-like stars. For $D \ll 1$, the pericentre distance to the central MBH becomes comparable to the tidal radius of the individual stars that compose the binary system. If the binary members are solar-type stars with its initial separation $a \sim 1$ au, they are tidally disrupted for $D \lesssim 5 \times 10^{-3}$. Such double tidal disruption events have been discussed by Mandel & Levin (2015). To achieve a deeper penetration without the disruption of the binary members, binaries need to have a wide initial separation, or they should consist of compact objects. We intend to provide the basic characteristics of the tidal encounter between binaries and a massive object in this paper. The tidal disruption of stellar mass BH binaries will be investigated in the context of BH mergers and LIGO observations (Fernandez et al., in preparation). Another possible implication of our results is the study of irregular satellites around giant planets, they follow a distant, inclined, and often eccentric and retrograde orbit. One of the leading mechanisms to produce such satellites is the three-body tidal encounter (Agnor & Hamilton 2006; Kobayashi et al. 2012).

We do not account for the possibility of stellar collisions during the tidal encounter. However, such collisions and the resultant mergers could have interesting consequences (Bradnick, Mandel & Levin 2017). We roughly evaluate the collision rate by using the parabolic restricted three-body approximation. Although the energy and disruption probability are accurately evaluated in this approximation, the separations of the binary members are overestimated for a short period around the periapsis passage $|t| < (m/M)^{1/3}\sqrt{a^3/Gm}$ for $D < (m/M)^{1/3}$ (Sari et al. 2010). If the mass ratio M/m is not very large, we might underestimate the collision rate. For $a/R_\star = 10$, where a is the initial binary separation and $R_\star$ is the radius of the binary members, we have evaluated the collision probability at the BH encounter as a function of D averaged over phase and orientation. If the minimum separation of binary members becomes less than $2R_\star$ during the evolution (or equivalently if it becomes less than 1/5 of the initial separation), we regard it as a collision case. We find that the collision probability is about 5–7 per cent for $D < 0.1$ and that the probability slightly increases at shallow encounters and it peaks around $D = 1.6$ with a peak value of ∼14 per cent. Even if collisions are taken into account, the disruption probability is very similar. Compared to the point particle results, the fractional difference $\Delta P_{\rm dis}/P_{\rm dis}$ is a few per cent for $D < 0.1$, and it peaks around $D = 1$ with $\Delta P_{\rm dis}/P_{\rm dis} \sim 5$ per cent. It means that most collision events are classified into the surviving case in the point particle calculations. $\Delta P_{\rm survive}/P$ is about 45 per cent for $D < 3 \times 10^{-2}$ (i.e. for deep penetrators, the surviving probability becomes about a half of the point particle value). $\Delta P_{\rm survive}/P_{\rm survive}$ gradually decreases for larger D and it is about 20 per cent for $D \sim 1$.

ACKNOWLEDGEMENTS

We thank the anonymous referee for valuable suggestions. This research was supported by STFC grants.

REFERENCES

Addison E., Laguna P., Larson S., 2015, preprint (arXiv:1501.07856)
Agnor C. B., Hamilton D. P., 2006, Nature, 441, 192
Alexander T., 2017, ARA&A, 55, 1
Antonini F., Faber J., Gualandris A., Merritt D., 2010, ApJ, 713, 90
Bradnick B., Mandel I., Levin Y., 2017, MNRAS, 469, 2042
Bromley B. C., Kenyon S. J., Geller M. J., Barcikowski E, Brown W. R., Kurtz M. J., 2006, ApJ, 653, 1194
Bromley B. C., Kenyon S. J., Geller M. J., Brown W. R., 2012, ApJ, 749, L42
Brown W. R., Geller M. J., Kenyon S. J., 2009, ApJ, 690, 1639
Brown W. R., Geller M. J., Kenyon S. J., 2012, ApJ, 751, 55
Brown W. R., Geller M. J., Kenyon S. J., 2014, ApJ, 787, 89
Ghez A. M. et al., 2008, ApJ, 689, 1044
Gillessen S., Eisenhauer F., Trippe S., Alexander T., Genzel R., Martins F., Ott T., 2009, ApJ, 692, 1075
Ginsburg I., Loeb A., 2006, MNRAS, 368, 221
Gualandris A., Portegies Zwart S., Sipior M. S., 2005, MNRAS, 363, 223
Hills J. G., 1988, Nature, 331, 687
Hills J. G., 1991, AJ, 102, 704
Kobayashi S., Hainick Y., Sari R., Rossi E. M., 2012, ApJ, 748, 105
Lu Y., Zhang F., Yu Q., 2010, ApJ, 709, 1356
Mandel I., Levin Y., 2015, ApJ, 805, L4
Miller M. C. Freitag M. Hamilton D. P., Lauburg V. M., 2005, ApJ, 631, L117
Perets H., Hopman C., Alexander T., 2007, ApJ, 656, 709

Perets H. B., Gualandris A., Kupi G., Merritt D., Alexander T., 2009, ApJ, 702, 884
Phahl E., 2005, ApJ, 626, 849
Rossi E. M., Kobayashi S., Sari R., 2014, ApJ, 795, 125
Rossi E. M., Marchetti T., Cacciato M., Kuiack M., Sari R., 2017, MNRAS, 467, 1844
Sari R., Kobayashi S., Rossi E. M., 2010, ApJ, 708, 605
Sesana A., Haardt F., Madau P., 2007, MNRAS, 379, L45
Yu Q., Tremaine S., 2003, ApJ, 599, 1129

This paper has been typeset from a TEX/LATEX file prepared by the author.